

# Core performance and mix in direct-drive spherical implosions with high uniformity\*

D. D. Meyerhofer,<sup>†,a)</sup> J. A. Delettrez, R. Epstein, V. Yu. Glebov, V. N. Goncharov, R. L. Keck, R. L. McCrory, P. W. McKenty, F. J. Marshall, P. B. Radha, S. P. Regan, S. Roberts, W. Seka, S. Skupsky, V. A. Smalyuk, C. Sorce, C. Stoeckl, J. M. Soures, R. P. J. Town, B. Yaakobi, and J. D. Zuegel  
*Laboratory for Laser Energetics, University of Rochester, 250 East River Road, Rochester, New York 14623-1299*

J. Frenje, C. K. Li, R. D. Petrasso,<sup>b)</sup> and F. H. Séguin  
*Plasma Fusion Center, Massachusetts Institute of Technology, Cambridge, Massachusetts 02139*

K. Fletcher, S. Padalino, and C. Freeman  
*SUNY Geneseo, Geneseo, New York 14454*

N. Izumi, R. Lerche, T. W. Phillips, and T. C. Sangster  
*Lawrence Livermore National Laboratory, Livermore, California 94550*

(Received 23 October 2000; accepted 26 December 2000)

The performance of gas-filled, plastic-shell implosions has significantly improved with advances in on-target uniformity on the 60-beam OMEGA laser system [T. R. Boehly, D. L. Brown, R. S. Craxton *et al.*, *Opt. Commun.* **133**, 495 (1997)]. Polarization smoothing (PS) with birefringent wedges and 1-THz-bandwidth smoothing by spectral dispersion (SSD) have been installed on OMEGA. The beam-to-beam power imbalance is  $\leq 5\%$  rms. Implosions of 20- $\mu\text{m}$ -thick CH shells (15 atm fill) using full beam smoothing (1-THz SSD and PS) have primary neutron yields and fuel areal densities that are  $\sim 70\%$  larger than those driven with 0.35-THz SSD without PS. They also produce  $\sim 35\%$  of the predicted one-dimensional neutron yield. The results described here suggest that individual-beam nonuniformity is no longer the primary cause of nonideal target performance. A highly constrained model of the core conditions and fuel-shell mix has been developed. It suggests that there is a “clean” fuel region, surrounded by a mixed region, that accounts for half of the fuel areal density. © 2001 American Institute of Physics.

[DOI: 10.1063/1.1350964]

## I. INTRODUCTION

In the direct-drive approach to laser-driven inertial confinement fusion (ICF)<sup>1</sup> a spherical target is symmetrically illuminated by a number of individual laser beams. One of the primary determinants of target performance is illumination uniformity, both individual-beam uniformity and on-target beam-to-beam power history differences (power balance). Illumination nonuniformities lead to distortions in the compressed core due to secular growth of low-order ( $l \leq 10$ ) modes and shell breakup and mix due to the Rayleigh–Taylor (RT)<sup>2,3</sup> growth of perturbations imprinted by high-order ( $l > 10$ ) nonuniformities. To reduce the effect of imprinting, a number of beam-smoothing techniques have been employed, including distributed phase plates (DPP),<sup>4</sup> polarization smoothing (PS) with birefringent wedges,<sup>5</sup> smoothing by spectral dispersion (SSD),<sup>6</sup> and induced spatial

incoherence (ISI).<sup>7</sup> Ultimately to ignite a direct-drive cryogenic pellet, the on-target beam nonuniformity must be less than 1%.<sup>3,8,9</sup>

An ICF target is RT unstable during two phases of the implosion: During the acceleration phase, surface nonuniformities seeded by laser nonuniformities, outer-target-surface roughness, and feedout of inner-target-surface roughness grow at the ablation front. Under extreme conditions, the perturbations can grow to be comparable to the in-flight shell thickness disrupting the shell or by feeding perturbations through the remaining shell material, seeding the deceleration-phase RT instability. During the deceleration and core assembly phases the boundary between the high-temperature, low-density hot spot and the colder, high-density pusher (shell) is RT unstable.

The beam uniformity's effect on target performance is studied in direct-drive implosions of gas-filled plastic shells on the OMEGA laser system.<sup>10</sup> These targets are surrogates<sup>11,12</sup> for cryogenic implosions that have recently commenced on OMEGA. These cryogenic implosions are energy-scaled surrogates for direct-drive ignition targets on the National Ignition Facility.<sup>3,8,9,13</sup> Cryogenic-target implosions have been shown to produce high fuel areal densities

\*Paper BI3 3, *Bull. Am. Phys. Soc.* **45**, 22 (2000).

<sup>†</sup>Invited speaker.

<sup>a)</sup>Also at the Departments of Mechanical Engineering and Physics and Astronomy, University of Rochester, Rochester, New York; electronic mail: ddm@lle.rochester.edu

<sup>b)</sup>Visiting Senior Scientist, Laboratory for Laser Energetics.

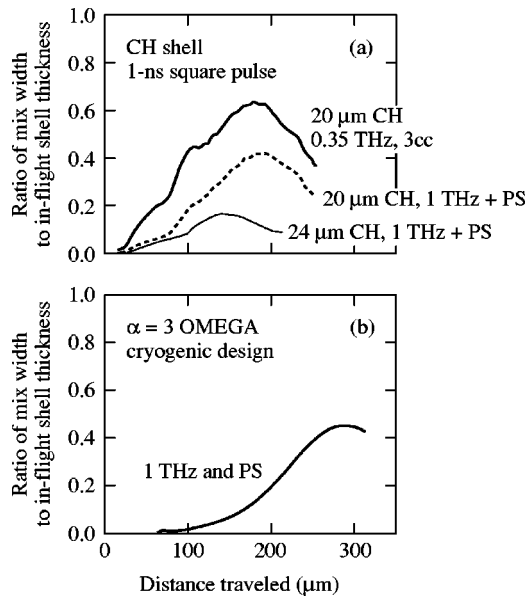


FIG. 1. (a) Ratio of the calculated acceleration phase “mix” width to the in-flight shell thickness for 20- $\mu\text{m}$ -thick CH shells illuminated by 1-ns square pulses with 1-THz SSD and PS (dashed line); 0.35-THz, three-color-cycle SSD without PS (thick solid line); and for a 24- $\mu\text{m}$ -thick CH shell illuminated with 1-THz SSD and PS (thin solid line). For full smoothing, the width of the mix region is significantly smaller than the in-flight shell thickness. (b) A similar comparison for NIF-scaled cryogenic targets planned for OMEGA is shown.

on the 24-beam OMEGA laser system<sup>14</sup> and the 12-beam GEKKO laser system.<sup>15</sup>

An important measure of target stability during the acceleration phase is the ratio of the amplitude of the ablation-surface mix width to the in-flight shell thickness. The smaller this ratio, the more stable the implosion. Figure 1 shows this ratio calculated for three different plastic-shell implosion conditions [Fig. 1(a)] and for a cryogenic-target implosion planned for OMEGA [Fig. 1(b)]. The in-flight shell thickness was calculated using the 1-D hydrodynamic code LILAC,<sup>16</sup> and the mix width was calculated using a postprocessor that includes the effects of mass ablation, finite shell thickness, and spherical convergence.<sup>17</sup> In implosions of 20- $\mu\text{m}$ -thick, gas-filled plastic shells driven with a 1-ns square laser pulse, the ratios of the thickness of the ablation-surface mix region due to RT growth to the in-flight shell thickness are similar to those predicted for OMEGA cryogenic implosions. The other two plastic-shell implosion conditions will be discussed below. Plastic shells are advantageous because a wide variety of shell/gas conditions and diagnostics can be applied to study the details of the implosion.<sup>18–20</sup>

In this paper we describe a series of OMEGA direct-drive plastic-shell implosions with high-quality beam smoothing and power balance. These experiments suggest that the shell remains reasonably integral during the acceleration phase and that single-beam nonuniformity is no longer the primary limitation on target performance. A wide variety of target types and fill gasses are used to build a model of core conditions and fuel-shell mixing.

In Sec. II we describe the targets and diagnostics applied to the spherical implosions. In Sec. III we describe the laser

conditions for the implosions; Sec. IV the target performance; and Sec. V a static mix model. The paper is summarized in Sec. VI.

## II. TARGETS AND DIAGNOSTICS

The philosophy of the experiments reported here is to first choose a laser pulse shape, smoothing conditions, target-shell thickness, and gas-fill pressure, and then vary the make-up of the fill gas or details of the shell layers so that many diagnostics can be applied to the nearly identical implosions. OMEGA produces very reproducible implosions suggesting that the implosion hydrodynamics is unchanged for different target types and fill-gas make-up.

### A. Core diagnostics

The primary ( $N_p$ ) and secondary neutron ( $N_s$ ) yields were measured using scintillator counters coupled to fast photomultipliers.<sup>21</sup> Indium and copper activation provided additional yield measurements.<sup>22</sup> For the range of yields recorded, the typical uncertainty in these measurements was 10%. The fast scintillator counters also measured the neutron averaged ion temperature with an uncertainty of  $\sim 0.5$  keV.

The secondary proton and knock-on particle yields were measured with filtered range filters<sup>23</sup> and charged-particle spectrometers (CPS).<sup>24</sup> CR-39 nuclear emulsion was used in both detectors to determine the yield and the energy spectrum.

For DT-filled implosions, the fuel areal density is determined from the number of elastically scattered knock-on fuel particles:<sup>25,26</sup>



The yield of knock-on particles is insensitive to the electron temperature profile.<sup>25,26</sup>

Limits on fuel areal density ( $\rho R_f$ ) in  $D_2$ -filled implosions can be inferred from the secondary neutron ( $N_s$ ) production,<sup>23,27</sup>



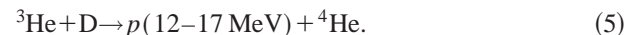
followed by



and secondary proton production ( $p_s$ ),<sup>23,27</sup>



followed by



The secondary proton and neutron yields depend on the electron temperature profile in the core and typically provide limits on the  $\rho R_f$  and the core electron temperature.<sup>23,27</sup>

The inferred value of  $\rho R_f$  depends on whether a hot spot (point-like source surrounded by uniform fuel) or uniform (uniform fuel and source) “ice-block” model is used. The  $\rho R_f$  inferred with the uniform model is  $\sim 34\%$  larger than with the hot-spot model.<sup>23,27</sup> Simulations using LILAC<sup>16</sup> suggest that the uniform model is more appropriate for inferring  $\rho R_f$  under the experimental conditions described in this work.

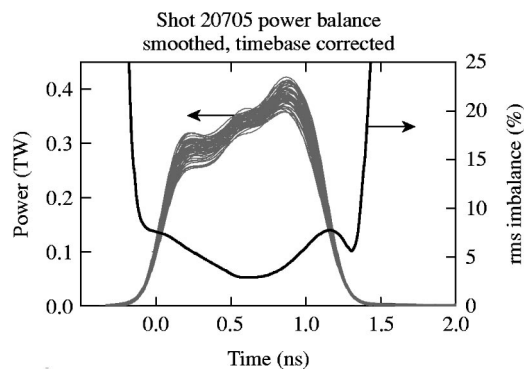


FIG. 2. The measured 1-ns square pulse from 50 of the 60 OMEGA beams for shot 20705 (thin solid lines). The thick solid line shows the rms beam-to-beam power imbalance inferred for the same shot. For most of the pulse, the power imbalance is  $\sim 5\%$ .

## B. Shell diagnostics

The areal density of the plastic shell,  $\rho R_s$ , during stagnation was measured with charged particle spectroscopy. Secondary protons from  $D_2$  implosions (produced with 12- to 17-MeV energies) are slowed down predominantly in the shell by an amount proportional to  $\rho R_s$ .<sup>23</sup> For CH shells with DT fill, the number of knock-on protons determines  $\rho R_s$ .<sup>26</sup> In addition, knock-on deuterons and tritons are slowed in the shell, providing another measure of  $\rho R_s$  and, coupled with the knock-on proton yield, provide an estimate of the shell electron temperature.<sup>26</sup>

## C. Mix diagnostics

The core-fuel mix characteristics are inferred in a number of ways. CD layers in  $D_2$ -filled CH targets are probed with tritons and  $^3\text{He}$  particles produced in the  $D_2$  reaction in the fuel region [Eqs. (2)–(5)].<sup>28</sup> The measured secondary yields from the shell regions are compared to 1-D simulations. When the yields are significantly different than those predicted, they provide information about the fuel-shell mix. The secondary DT neutrons and  $D$ - $^3\text{He}$  protons produced directly in the shell can be subtracted using  $H_2$ -filled implosions with the same shell conditions. An implosion of a plastic shell with a CD layer and a pure- $^3\text{He}$  fill provides a primary  $D$ - $^3\text{He}$  proton signal only if the shell and fuel regions are microscopically mixed. This yield depends on the characteristics of the mix, either microscopic (diffusive) or macroscopic, where islands of shell material penetrate the core.

## III. LASER CONDITIONS

A  $\sim 23$ -kJ, 1-ns square pulse delivered by the 60-beam OMEGA laser system<sup>10</sup> was used to drive the implosions described in this work. Figure 2 shows the measured pulse shapes for 50 (of the 60) beams. The beam-to-beam UV energy balance (the thick line in Fig. 2) is typically  $\leq 5\%$  rms. When beam overlap on the target is included, the on-target nonuniformity due to beam-to-beam power imbalance is  $< 2\%$  ( $l \leq 12$ ). Individual-beam smoothing was accomplished by combining DPP's, SSD, and PS (in most cases). The DPP's produce a third-order super-Gaussian pro-

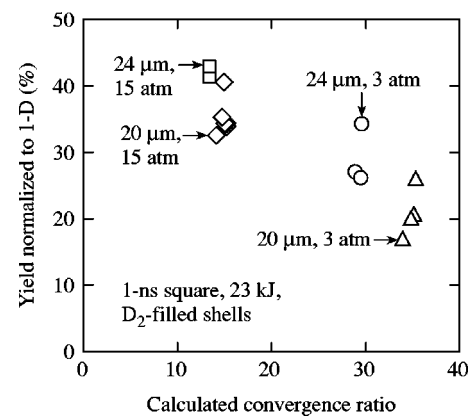


FIG. 3. Ratio of the measured to calculated primary neutron yield (YOC) for  $D_2$ -filled CH capsule implosions as a function of calculated convergence ratio for 1-THz SSD and PS. This shows both the high reproducibility of the OMEGA laser system and good performance at convergence ratios of  $\sim 35$ .

file with 95% of the energy enclosed in an  $\sim 936$ - $\mu\text{m}$  diameter. When 2-D SSD and PS are added, the spot diameter increases somewhat due to the angular divergence associated with these techniques. Two different two-dimensional (2-D) SSD configurations were used: a single color cycle with 1-THz bandwidth at 3- and 10-GHz modulation frequencies or a three-color-cycle configuration with a 0.35-THz bandwidth with 3- and 3.3-GHz modulation frequencies. Polarization smoothing with birefringent wedges was employed on the implosions with 1-THz SSD.

The calculated time-dependent, on-target nonuniformity ( $l = 1 - 500$ ) due to single-beam nonuniformity assuming a perfect beam-to-beam power balance for 1-THz SSD with PS is less than 1% after 300 ps.<sup>29</sup> Additional on-target nonuniformities are due to beam-to-beam power imbalance and differences in DPP spot sizes.

## IV. IMPLOSION RESULTS

In this section we describe a series of gas-filled plastic (CH) shell implosions driven with a  $\sim 23$  kJ, 1-ns square pulse. Most of the implosions were driven with full beam uniformity (1-THz SSD and PS), while 0.35-THz SSD (three color cycles without PS) was used for the others. The  $\sim 940$ - $\mu\text{m}$ -diam plastic targets had 18–24- $\mu\text{m}$  wall thicknesses and were filled with fuel pressures of 3–15 atm. The targets were predicted to have gas convergence ratios of  $\sim 35$  and  $\sim 14$ , respectively, from 1-D hydrodynamic simulations.<sup>16</sup>

The ratio of the measured primary neutron yield to that predicted by 1-D simulations [“yield over clean” (YOC)] for CH shells with  $D_2$  fills as a function of the calculated convergence ratio (initial to final radius of the fuel-shell boundary) for 1-THz SSD and PS is shown in Fig. 3. The 20- and 24- $\mu\text{m}$ -thick shells were filled with either 3 or 15 atm of  $D_2$ . The OMEGA laser system provides highly reproducible implosions, as can be seen by the small spread in the YOC's for each condition. The implosions with 15-atm-filled, 20- $\mu\text{m}$ -thick shells were taken over three experimental campaigns spanning two months and show an  $\sim 10\%$  standard deviation of YOC's. The implosions with convergence ratio

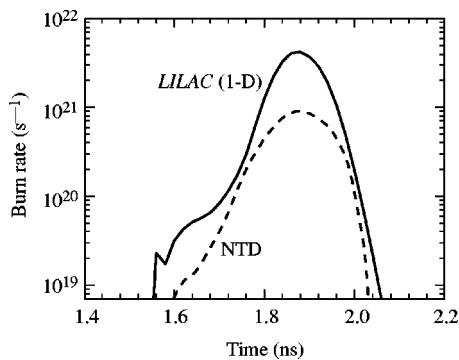


FIG. 4. The time-dependent, measured (dashed) and predicted (solid) neutron-production rates for a 15-atm-DT fill in a 20- $\mu\text{m}$ -thick CH shell are overlaid.

$\sim 35$  have YOC's of  $\sim 20\%$ . The most-stable implosions (24- $\mu\text{m}$ -thick shells with 15-atm fills) have YOC's  $\geq 40\%$ .

The measured and calculated neutron-production rates for a 20- $\mu\text{m}$ -thick CH shell filled with 15 atm of  $\text{D}_2$  are compared in Fig. 4. The two temporal histories are in good agreement except that the measured neutron-production rate is  $\sim 35\%$  of the calculated one. There is no evidence that the measured neutron burn rate decreases before the time predicted by 1-D simulations (i.e., no early burn termination). Over many target implosions, the measured time of peak neutron emission (bang time) is within 50 ps of that predicted.

For 20- $\mu\text{m}$ -thick CH shells with 15-atm- $\text{D}_2$  or DT fill pressures, the predicted  $\rho R_f$  is  $16 \text{ mg/cm}^2$  and  $\rho R_s$  is  $60 \text{ mg/cm}^2$ . The measured charged-particle spectra used to determine the fuel, shell, and total areal densities of these implosions are shown in Figs. 5–7. Figures 5 and 6 show the measured knock-on D and p spectra for CH shells filled with DT. The  $\rho R_f$  inferred from D knock-on yield is  $16 \text{ mg/cm}^2$ , while  $\rho R_s \sim 61 \text{ mg/cm}^2$  from the knock-on protons. The total  $\rho R$  can also be determined from the slowing down of  $\text{D-}^3\text{He}$  secondary protons from  $\text{D}_2$ -filled shells (Fig. 7) and it is found to be  $76 \text{ mg/cm}^2$ . These measurements show that the sum of fuel and shell areal densities for DT implosions is in good agreement with the total areal density independently inferred from  $\text{D}_2$  implosions. The measured fuel and shell areal densities are close to those predicted from 1-D simulations.

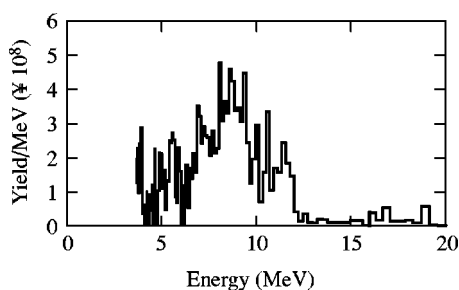


FIG. 5. The measured "knock-on" deuteron spectrum for a 15-atm-DT fill in a 20- $\mu\text{m}$ -thick CH shell. The estimated fuel areal density is  $16 \text{ mg/cm}^2$  (Ref. 26).

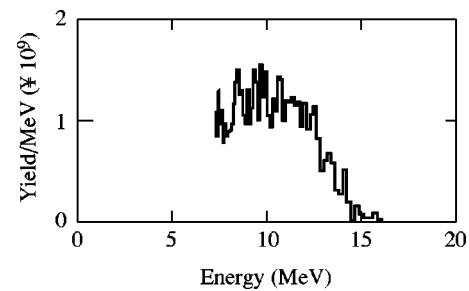


FIG. 6. The measured knock-on proton spectrum for a 15-atm-DT fill in a 20- $\mu\text{m}$ -thick CH shell. The estimated shell areal density is  $61 \text{ mg/cm}^2$  (Ref. 26).

These results were compared with target implosions driven with similar laser pulse shapes and with larger single-beam nonuniformities (0.35-THz, three-color-cycle SSD without PS). LILAC simulations predicted identical target performance. Table I compares the measured implosion parameters for 20- $\mu\text{m}$ -thick CH shells with 15-atm-gas fills of  $\text{D}_2$  and DT driven under identical conditions, except for the single-beam nonuniformity. In all aspects, the implosions driven with more-uniform beams performed significantly better. In particular both the primary neutron yield and fuel areal density increased by  $\sim 70\%$ .

In summary, high-uniformity, moderate-convergence-ratio implosions with 15-atm-gas-fill pressure have YOC's of  $\sim 40\%$  and compressed fuel and shell areal densities close to those predicted. Figure 1(a) shows the predicted ratio of the imprint-induced mix width to the shell thickness for three implosions. When full smoothing (1-THz SSD and PS) is applied to 20- $\mu\text{m}$ -thick shells, the mix width is predicted to be  $\sim 42\%$  of the in-flight shell thickness compared with 65% for 0.35-THz SSD without PS. The primary yields and fuel areal densities increased by  $\sim 70\%$  for the 1-THz and PS implosion, indicating that the reduction of mix width and corresponding improvement in shell stability significantly enhanced the target performance. The 24- $\mu\text{m}$ -thick CH shells with 15-atm fills show a further 25% improvement in YOC compared to 20- $\mu\text{m}$ -thick shells with full beam smoothing. If the imprint-induced shell stability were still the dominant determinant of target performance, reducing the ratio of the mix width to in-flight shell thickness from 42% to 17% might have been expected to improve target performance significantly further. While shell stability still plays a

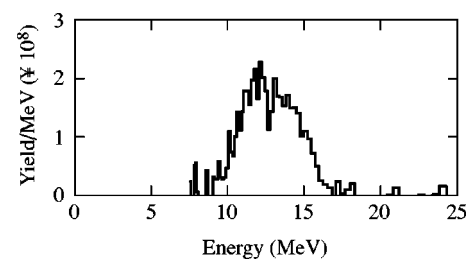


FIG. 7. The measured secondary  $\text{D-}^3\text{He}$  proton spectrum for a 15-atm- $\text{D}_2$  fill in a 20- $\mu\text{m}$ -thick CH shell. The estimated total areal density is  $76 \text{ mg/cm}^2$  (Ref. 23).

TABLE I. Comparison of implosion performance of  $\sim 19\text{-}\mu\text{m}$ -thick CH shells filled with 15 atm of  $\text{D}_2$  or DT fill with 1-THz SSD and PS or 0.35-THz SSD (three color cycles) without PS.

Diagnostic	0.35-THz SSD	1-THz SSD and PS
$\text{D}_2$ primary yield ( $10^{10}$ )	$9 \pm 1$	$16 \pm 1$
$T_{\text{ion}}(\text{D}_2)$	$3.2 \pm 0.5$ keV	$3.7 \pm 0.5$ keV
Secondary neutron ratio ( $Y_{2n}/Y_n$ ) ( $10^{-3}$ )	$1.5 \pm 0.4$	$2.5 \pm 0.2$
Secondary proton ratio ( $Y_{2p}/Y_n$ ) ( $10^{-3}$ )	$1.4 \pm 0.2$	$1.9 \pm 0.2$
DT primary yield ( $10^{12}$ )	$6 \pm 1$	$11 \pm 1$
$T_{\text{ion}}(\text{DT})$	3.7 keV	4.4 keV
Knock-on fuel $\rho R$ ( $\text{mg}/\text{cm}^2$ )	$9 \pm 2$	$15 \pm 2$

role in target performance, it appears that other effects, such as power imbalance play a comparable role.

**V. CORE MIX MODEL**

In the preceding sections, the experimental results have been compared with the predictions of 1-D hydrodynamic simulations. While some observations are close to those predicted, others, such as the primary yield, are lower, while still others, such as the ratio of the secondary neutron yield to the primary neutron yield, are larger. The variation in observables provides constraints on the possible core conditions and fuel–pusher mix during stagnation. In this section, the experimental results are compared to a static model of the core to gain additional insight about target performance.<sup>30</sup>

The predictions of this static model are compared to neutron-burn-averaged observations. This model assumes that the compressed core can be divided into two regions: a ‘‘clean’’ region with only fuel material and a ‘‘mixed region’’ where some of the shell material is mixed with the fuel material. The clean region is characterized by a single temperature (electron and ion are assumed to be the same), fuel density, and radius. In the mix region, the fuel density decreases linearly from the edge of the clean region to the edge of the mix region, the shell material density decreases linearly from the edge of the mix region to the boundary of the clean region, and the temperature decreases linearly from the edge of the clean region to the edge of the mix region. Thus, the model has six parameters: the temperature, density, and radius of the clean region, the radius of the mix region, and the shell material density and temperature at the edge of the mix region. The total fuel mass is assumed to be conserved. The nuclear and particle emission from the compressed core in the model must match the measured values of primary neutron burn rate, average neutron ion temperature, secondary neutron, proton, and knock-on yields (both for CH shells and CH shells with inner CD layers). CH shells with inner CD layers filled with  $^3\text{He}$  fuel provide additional experimental observations. Approximately ten experimental observables are used to constrain the model’s parameters. The core temperature and density profiles inferred from this model for 15-atm-filled,  $20\text{-}\mu\text{m}$ -thick plastic shells is shown in Fig. 8. The range of allowable parameters is shown in the figure as the width of parameter estimates. The measured values of various parameters and their fraction (in percent)

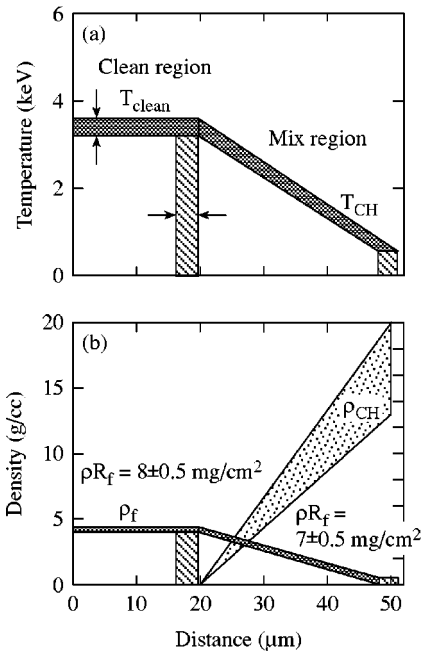


FIG. 8. Inferred core and fuel–shell mix profiles from the mix model described in the text. The temperature profiles are shown in (a) and the density profiles in (b). The range of the parameters, which are consistent with the experimental observations, is shown by the width of the various parameter bands.

predicted by the model are shown in Table II. The model predicts that the total compressed radius is  $50\ \mu\text{m}$  with approximately  $1\ \mu\text{m}$  (20% of the compressed shell areal density) of the original shell material mixed into the outer 50% of the fuel region. This model provides a picture of the stagnation conditions for the specifications described here. In the future it will be applied to other implosions to further understand the mix characteristics.

**VI. CONCLUSIONS**

In summary, the implementation of full beam smoothing (1-THz SSD and PS) on OMEGA has produced moderate-convergence-ratio ( $\text{CR} \sim 15$ ) implosions that perform close to 1-D predictions. The primary neutron yield is  $\sim 35\% - 45\%$  of that predicted, while the fuel and shell areal densities are close to their predicted values. When the shell is thickened to reduce the effect of the acceleration-phase RT

TABLE II. A comparison of measured and mix-model-predicted implosion parameters for  $\sim 19\text{-}\mu\text{m}$ -thick CH shells (with or without CD layers) filled with 15 atm of  $\text{D}_2$  or DT, or  $^3\text{He}$  for implosions with 1-THz SSD and PS.

Parameter	Measurement	Model (% of expt)
Fuel $\rho R$ ( $\text{mg}/\text{cm}^2$ )	$15 \pm 2$	100
$T_{\text{ion}}(\text{DT})$ (keV)	$4.4 \pm 0.4 \pm 0.5$ (sys)	86
Max: neutron burn rate (n/s)	$(9 \pm 1) \times 10^{20}$	110
$T_{\text{ion}}(\text{D}_2)$ (keV)	$3.7 \pm 0.2 \pm 0.5$ (sys)	89
Secondary neutron ratio	$(2.4 \pm 0.4) \times 10^{-3}$	100
Secondary proton ratio	$(1.8 \pm 0.3) \times 10^{-3}$	78
Secondary neutron ratio ( $\text{D}_2$ )	$(3.1 \pm 0.5) \times 10^{-3}$	94
D- $^3\text{He}$ proton yield ( $^3\text{He}$ fill)	$(1.3 \pm 0.2) \times 10^7$	66
$\text{D}_2$ neutron yield ( $^3\text{He}$ fill)	$(8.5 \pm 0.4) \times 10^8$	97

instability, the performance improves only slightly, suggesting that single beam nonuniformities are no longer the dominant determinant of target performance. The stagnation conditions are reproduced by a tightly constrained static mix-model.

Future research will address the effect of residual beam-to-beam power imbalances and target manufacturing nonuniformities as limitations of target performance. Implosions that are less stable during the acceleration phase (e.g., more slowly rising pulses) will be used to further understand the fuel-shell mixing. In addition, x-ray diagnostics will be utilized and their results compared to the static mix model.

Cryogenic-target implosions have begun on the OMEGA laser system. An ignition target on a MJ-class laser system such as the National Ignition Facility will require a shell composed primarily of a frozen DT layer. The OMEGA experiments are energy-scaled versions of ignition implosions with  $\sim 100\text{-}\mu\text{m}$ -thick ice layers. The stability properties of these targets due to imprinting are similar to those described in this paper. The results described here lead to confidence in the ability to obtain the direct-drive ignition on the National Ignition Facility.<sup>8</sup>

## ACKNOWLEDGMENTS

The authors are extremely grateful to the staff of the Laboratory for Laser Energetics for their dedicated efforts in developing and providing the high-performance OMEGA laser system, including low power imbalance and high single-beam uniformity, and high-quality diagnostics, operations, and target fabrication.

This work was supported by the U.S. Department of Energy (DOE) Office of Inertial Confinement Fusion under Cooperative Agreement No. DE-FC03-92SF19460, the University of Rochester, and the New York State Energy Research and Development Authority. The support of the DOE does not constitute an endorsement by the DOE of the views expressed in this article.

<sup>1</sup>J. Nuckolls, L. Wood, and A. Thiessen *et al.*, *Nature (London)* **239**, 139 (1972).

<sup>2</sup>J. D. Kilkenny, S. G. Glendinning, S. W. Haan *et al.*, *Phys. Plasmas* **1**, 1379 (1994).

<sup>3</sup>S. E. Bodner, D. G. Colombant, J. H. Gardner *et al.*, *Phys. Plasmas* **5**, 1901 (1998).

<sup>4</sup>T. J. Kessler, Y. Lin, J. J. Armstrong *et al.*, in *Laser Coherence Control: Technology and Applications*, edited by H. T. Powell and T. J. Kessler (SPIE, Bellingham, WA, 1993), Vol. 1870, pp. 95–104.

<sup>5</sup>T. R. Boehly, V. A. Smalyuk, D. D. Meyerhofer *et al.*, *J. Appl. Phys.* **85**, 3444 (1999).

<sup>6</sup>S. Skupsky, R. W. Short, T. Kessler *et al.*, *J. Appl. Phys.* **66**, 3456 (1989).

<sup>7</sup>R. H. Lehmburg and S. P. Obenshain, *Opt. Commun.* **46**, 27 (1983).

<sup>8</sup>P. W. McKenty, V. N. Goncharov, R. P. J. Town *et al.*, *Phys. Plasmas* **8**, 2315 (2001).

<sup>9</sup>See National Technical Information Service Document No. UCRL-LR-105821-97-2, S. V. Weber, D. Eimerl, J. E. Rothenberg *et al.*, "Direct-drive capsules for NIF," ICF Quarterly Report, Lawrence Livermore National Laboratory, Livermore, CA, 1997, Vol. 7, Issue 2, P. 43. Copies may be ordered from the National Technical Information Service, Springfield, VA 22101.

<sup>10</sup>T. R. Boehly, D. L. Brown, R. S. Craxton *et al.*, *Opt. Commun.* **133**, 495 (1997).

<sup>11</sup>F. J. Marshall, J. A. Delettrez, V. Yu. Glebov *et al.*, *Phys. Plasmas* **7**, 1006 (2000).

<sup>12</sup>J. A. Delettrez, V. Yu. Glebov, F. J. Marshall *et al.*, *Bull. Am. Phys. Soc.* **44**, 192 (1999).

<sup>13</sup>C. P. Verdon, *Bull. Am. Phys. Soc.* **38**, 2010 (1993).

<sup>14</sup>F. J. Marshall, S. A. Letzring, C. P. Verdon *et al.*, *Phys. Rev. A* **40**, 2547 (1989).

<sup>15</sup>K. A. Tanaka, T. Yamanaka, K. Nishihara *et al.*, *Phys. Plasmas* **2**, 2495 (1995).

<sup>16</sup>M. C. Richardson, P. W. McKenty, and F. J. Marshall *et al.*, in *Laser Interaction and Related Plasma Phenomena*, edited by H. Hora and G. H. Miley (Plenum, New York, 1986), Vol. 7, pp. 421–448.

<sup>17</sup>V. N. Goncharov, P. McKenty, S. Skupsky *et al.*, *Phys. Plasmas* **7**, 5118 (2000).

<sup>18</sup>M. D. Cable, S. P. Hatchett, J. A. Caird *et al.*, *Phys. Rev. Lett.* **73**, 2316 (1994).

<sup>19</sup>D. K. Bradley, J. A. Delettrez, R. Epstein *et al.*, *Phys. Plasmas* **5**, 1870 (1998).

<sup>20</sup>F. J. Marshall, J. A. Delettrez, R. Epstein *et al.*, *Phys. Plasmas* **7**, 2108 (2000).

<sup>21</sup>V. Yu. Glebov, D. D. Meyerhofer, C. Stoeckl *et al.*, *Rev. Sci. Instrum.* **72**, 1 (2001).

<sup>22</sup>See National Technical Information Service Document No. UCRL-50021-86, S. M. Lane, B. A. Jones, N. J. Selchow *et al.*, "Neutron activation yield detectors," *Laser Program Annual Report 1986*, Lawrence Livermore National Laboratory, Livermore, CA, 3-100, 1987. Copies may be ordered from the National Technical Information Service, Springfield, VA 22101.

<sup>23</sup>F. H. Séguin, C. K. Li, and D. G. Hicks *et al.*, "Using secondary proton spectra to study imploded D<sub>2</sub>-filled capsules at the OMEGA laser facility," submitted to *Phys. Plasmas*.

<sup>24</sup>D. G. Hicks, Ph.D. thesis, Massachusetts Institute of Technology, 1999.

<sup>25</sup>S. Skupsky and S. Kacemjar, *J. Appl. Phys.* **52**, 2608 (1981).

<sup>26</sup>C. K. Li, D. G. Hicks, H. Séguin *et al.*, "Study of direct-drive, DT gas-filled-plastic capsule implosions using nuclear diagnostics on OMEGA," submitted to *Phys. Plasmas*.

<sup>27</sup>H. Azechi, M. D. Cable, and R. O. Stapf, *Laser Part. Beams* **9**, 119 (1991).

<sup>28</sup>V. Yu. Glebov, J. A. Delettrez, R. Epstein *et al.*, *Bull. Am. Phys. Soc.* **44**, 194 (1999).

<sup>29</sup>S. Skupsky and R. S. Craxton, *Phys. Plasmas* **6**, 2157 (1999).

<sup>30</sup>P. B. Radha, V. Yu. Glebov, F. J. Marshall *et al.*, *Bull. Am. Phys. Soc.* **45**, 164 (2000).